Variations in Thickness of the Upper Mantle Transition Zone

Yu J. Gu, Adam M. Dziewonski
gu@seismology.harvard.edu, dziewons@seismology.harvard.edu
Department of Earth and Planetary Sciences, Harvard University, MASS, USA.

Abstract

We analyze recordings from more than 3,000 shallow earthquakes and measure the $S410S - S660S$ differential travel times on the global scale. These differential times are obtained using a cross-correlation technique that minimizes effects associated with *a priori* assumptions of crustal thickness and velocity variations above the transition zone. Our measurements show absolute perturbations up to 8 seconds from the global average, which imply lateral variations of ±20 km in transition zone thickness, on the length scale over 2,000 km. This range of variations is consistent with those reported by earlier studies of SS precursors (e.g., Flanagan and Shearer, 1998; Gu et al., 1998), but is significantly larger than a recent result from P-to-S converted waves (Chevrot et al., 1999). The transition zone under major subduction zones, e.g., western Pacific and South America, is significantly thicker than global average, which indicates the strong thermal influence of subducted slabs. Anomalously thin transition zone is observed in the central Pacific, northern Atlantic and South Africa. We also observe a slight negative correlation between the $S410S-S660S$ times and the predicted S-travel time perturbations in the transition zone; this implies that large-scale topographic variations of the transition zone discontinuities are considerably affected by variations in temperature. A regional analysis shows a continent–ocean difference, i.e., the transition zone is generally thicker under continents than under oceans, though we do not see a clear correlation of thickness with age.

1. The issue of a debate

A number of studies of secondary phases have provided regional and global constraints on the thickness of the upper mantle transition zone. For example, Dueker and Sheehan (1997) observed a local thickness of 241 km across the Yellowstone hotspot track with absolute variations greater than 20 km. Gu et al. (1998) analyzed a large collection of SS precursors and obtained an average transition zone thickness of ∼240 km, with perturbations in excess of ±25 km on the global scale; these estimates were supported by the results of Flanagan and Shearer (1998) from a similar but slightly smaller data set. Gossler and Kind (1996) found a correlation between thickness of the transition zone and surface tectonics, thus suggesting that deep roots of continents may extend into the upper mantle transition zone.

The accuracy of these results were questioned, however, by a recent study using P-to-S converted waves (Chevrot et al. 1999). This study combined new and some existing measurements of Pds, and concludes that the transition zone is "flat" (with absolute lateral variations < 10 km) on the global scale. In addition, in areas where the Pds observations overlap with the former SS precursor observations, discrepancies of up to 15 km in predicted transition zone thickness are observed. The global average thickness of the transition zone, as inferred from Pds, is more than 8 kilometers thicker than that obtained by the SS precursors. Such large disagreements from using two different data sets require further explanation.

We do recognize that there is a significant difference in the resolution of the SdS and Pds phases in terms of imaging transition zone thickness. Our study, like the others that use SS precursors, is not aimed at the short wavelength structure associated, for example, with the topography of the 660 km discontinuity in the immediate vicinity of a subducted slab (e.g., Wicks and Richards, 1993). The size of the half-period Fresnel zone is on the order of $1,500$—$2,000$ km, and hence such small-scale perturbations would be averaged out or strongly attenuated. Our resolution will also be limited at short wavelength because the size of the averaging cap (10°) implies an effective low-pass filtering with a corners at about $\ell = 10$, or the half-wavelength of about 2,000 km. The half-period Fresnel zone of a 6-second P-to-S converted wave, on the other hand, has an oval shape and a diameter of 200–300 km. This means that most of the long-wavelength topography on the transition zone discontinuities, imaged by SS precursors, has little effect on the travel times of Pds. Difference in the lateral resolution of these two types of phases could, and should in theory, account for part of the discrepancy between the results of P-to-S converted waves and that of SS precursors.

The rapid increase in the number of good quality stations from the global seismographic network in recent years, as well as the need to improve the modeling techniques, provide motivations for us to undertake a new global study of transition zone thickness.

2. Data and method

We examine the travel times of SS precursors using high quality broad-band and long-period transverse com-

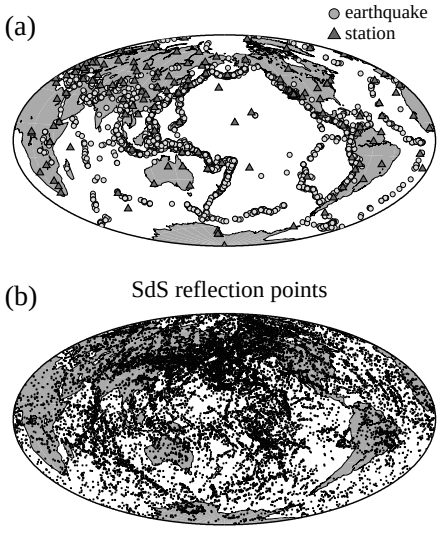

Figure 1: (a) Locations of 3021 shallow earthquakes (circles) and 130 stations from GDSN, GEOSCOPE, MEDNET and other seismic networks around the world (triangles). This data set produces more than 20,000 SH-component seismograms for our study. (b) Ray theoretical reflection points of 21,042 high quality SS precursors.

ponent seismograms. Our data set includes recordings collected by GDSN, IRIS, GEOSCOPE, and other seismic networks from earthquakes between 1989 and 2000 (Figure 1a). Our final data set contains ∼17,000 high quality SH-component seismograms after automatic and manual selections; this compares favorably to the ∼2900 Pds observations compiled by Chevrot et al. (1999). Many of the new SS reflection points fall in previously undersampled regions by Gu et al. (1998), e.g., in South America, the southern Pacific, Atlantic and Indian oceans (Figure 1b).

Global measurements of transition zone thickness have traditionally relied on the determination of the topography on the 410- and 660-km discontinuities. Effectively transition zone thickness is obtained by simple subtraction of the depths of the 410- and 660-km discontinuities. Because this is an indirect measurement, the accuracy of the resulting transition zone thickness is affected by the accuracy of the individual discontinuity depths; potential errors in the analysis of either discontinuity (due to the lack of data coverage or complexities in the transition zone) can potentially accumulate and influence the result of transition zone thickness. Alternatively, instead of solving for the topography of the 410- and 660-km boundaries separately, we exploit the similarity between the $S410S$ and $S660S$ waveforms and measure their differential travel times directly using a cross-correlation technique.

The first step of our approach involves finding the best phase window that encloses the waveform of $S660S$. To achieve this move-out corrections for epicentral distance must be applied in order to best align the $S660S$ phase. Then a common phase window is used to compute the autocorrelation function with each corresponding seismogram. Figures 2a and 2b show a series of synthetic (calculated using PREM; Dziewonski and Anderson, 1981) and data correlation functions after the $S660S$ waveforms have been correlated with the respective seismograms. The peak that is labeled *660* represents the beginning of the correlation window. The second peak, which is pronounced in the synthetics, is rather subtle in the data profile. After stacking of these correlation functions, the $S410S - S660S$ travel time residual (relative to that predicted by PREM) is simply the travel time difference between the observed and synthetic correlation peaks that correspond to a 410-km reflection (Figure 2c). This approach essentially removes the potential errors associated with the *a priori* assumptions of mantle heterogeneities above the transition zone, and of variations in crustal thickness and free-surface topography, since the $S410S - S660S$ times are essentially insensitive to these effects.

3. Global $S410S - S660S$ residuals

The differential travel time of $S410S - S660S$ mainly originates from the boundary topography of the 410- and 660-km discontinuities in combination with transition zone heterogeneities near the reflection points. A global map of $S410S - S660S$ travel time residuals, without correcting for velocity perturbations in the transition zone, is shown in Figure 3. An average residual of -8.1 s relative to the travel time predicted by PREM is removed from the residuals, and the values are interpolated using a degree 12 spherical harmonic expansion. Significant positive perturbations relative to the global average, shown in blue, are observed under the western Pacific and Eurasia, South Atlantic, and North America. In particular, anomalies with perturbations greater than 8 s and lateral dimensions larger than 3,000 km are present under the western Pacific and African Rift Zone. The locations and dimensions of these anomalies follow closely the fast velocities in the transition zone. Negative perturbations of significant lateral scale are present under the Pacific and northern Atlantic. Sample correlation functions in Figure 3 show variations from -6 s to 7 s from the predicted times of $S410S - S660S$ using PREM. The correlation peak that corresponds to the underside reflection of $S410S$ vary greatly both in shape and arrival time from region to region; this suggests a high level of complexity on topography of the transition zone discontinuities.

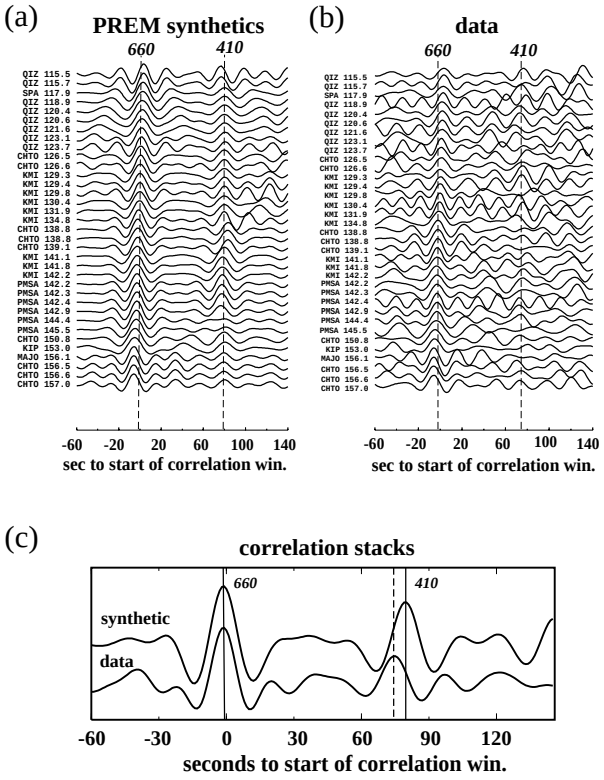

Figure 2: Autocorrelation functions produced by correlating the $S660S$ phase window with the respective seismograms for: (a) synthetics, and (b) observations. Moveout corrections for $S410S - S660S$ are subsequently applied to both the observed and synthetic autocorrelation functions. (c) Autocorrelation stacks. Travel time residual of $S410S - S660S$ can be readily measured from the travel time difference between the observed (dotted vertical line) and synthetic (solid line) autocorrelation peaks associated with the 410 km discontinuity.

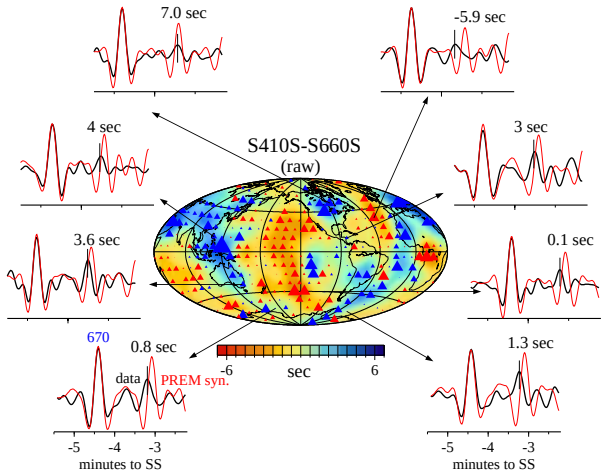

Figure 3: A global map of $S410S - S660S$ without correcting for the velocity variations within the transition zone. Red triangles represent thinner transition zone than the global average, and blue triangles, thicker transition zone. The thickness values are interpolated using a degree 12 spherical harmonic expansion. Sample waveforms for the stacked synthetic and data autocorrelation functions are shown in red and black, respectively. Short black lines denote the correlation peaks associated with the 410-km reflection on the data stacks. The marked times denote the residuals between the observed and predicted $S410S - S660S$ relative to the global average of -8.1 s. The arrows show the location of the respective autocorrelation functions.

4. Global transition zone thickness

To convert the corrected differential travel times of $S410S - S660S$ into thickness variations of the transition zone, we express the boundary undulation for a reflected wave as

$$\delta h_i = \frac{\delta t_i r_i}{2(\eta_i^2 - p_i^2)^{\frac{1}{2}}}, \qquad (1)$$

where i represents a given discontinuity, $\eta_i = r_i/v(r_i)$ and p_i is the ray parameter (Dziewonski and Gilbert, 1976). We use a ray parameter of 12.0 and 11.8 s/° for the 410- and 660-km discontinuities, respectively, assuming reflected waves at an epicentral distance of 130°.

Using this approach we obtain an average transition zone thickness of 241.7 km; this agrees well with Flanagan and Shearer (1998; 241 km) and Gu et al. (1998; 242 km), but is significantly thinner than that of Chevrot et al. (1999; 250 km). A comparison of the thickness maps inferred from SS precursors is shown in Figure 4. To first order, the global pattern of the long wavelength variations obtained from this study (Figure 4a) are consistent with those of the earlier results (Figures 4b and 4c). All three maps show significantly increased thickness in the Northwest Pacific, Indonesia and western Europe, and decreased thickness in the cental Pacific and Africa. It is encouraging that the main features of this study are notably more coherent laterally than the earlier studies; this may imply more effective cap averaging, owing mostly to improved data coverage on the global scale. Regional differences do exist, however, most notably in the amplitude of the variations; for example, our new measurements show less pronounced variations in the western Pacific than Gu et al. (1998). This difference may originate in part from the more restrictive data coverage of that earlier study, and in part, from the complexities in the topography of 400- and 660-km discontinuities near a

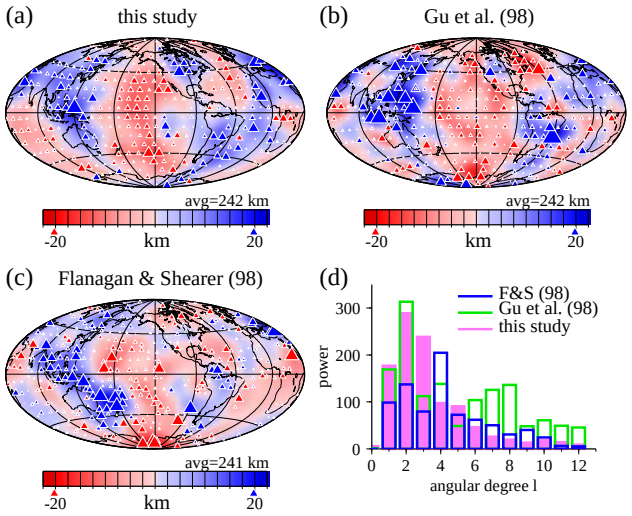

Figure 4: Thickness maps of the transition zone. In all maps, the residuals are interpolated using a spherical harmonic expansion up to the degree 12 (plotted on the background); an increased thickness from the global average is shown in blue, and a decrease thickness, in red. (a) Thickness variations inferred from $S410S - S660S$ of this study. (b) Thickness variations of Gu et al. (1998), inferred from SS-SdS. (c) Thickness variations of Flanagan and Shearer (1998), inferred from SS-SdS. Only caps with more than 20 records are plotted. (d) Power spectra of the three thickness maps. The long-wavelength features are fairly consistent among these maps which are dominated by low-degree harmonics.

subduction zone. Another significant difference is evident in New Zealand and Tonga-Kermadec, where Flanagan and Shearer (1998; Figure 4b) shows a markedly thicker transition zone than the other two studies. This discrepancy could be related to the higher uncertainties of the measurements in this region (see Figure 4a). Regardless of these regional differences, however, the overall agreement in the large-scale patterns of transition zone thickness illustrates the robustness of our technique and the reliability of the measurements. The power spectra of these three maps (Figure 4d) show strong signatures at the low-degree spherical harmonics; our new measurements are dominated by degrees $1 - 3$, and the spectral amplitudes at degrees 1 and 2 correlate well with those of Gu et al. (1998). In comparison, the spectral amplitude of Flanagan and Shearer (1998) are slightly smaller, though low degrees such as degrees 2 and 4 are still important signals in their analysis.

5. Regional thickness variations

One of the most intriguing puzzles in mantle dynamics is the depth to which the continental lithosphere is distinct in the upper mantle. Results obtained from global seismic tomography show that continent and ocean differences persist at least down to 250 km, and perhaps deeper. Studies using secondary reflected and converted phases have provided direct evidence of the depth extent of surface tectonics. Gossler and Kind (1996) point out that the transition zone is nearly 14 km thicker under Asian and North American continents than underneath the neighboring Pacific ocean, thus suggesting deep roots of the major continents. Gu et al. (1998) report regional variations in the occurrence of the 520-km discontinuity, from which the reflected waves are significantly more pronounced under intermediate-aged oceans than they are under the North American and African shields.

Gurrola and Minster (1998) reported a transition zone thickness variation exceeding 30 km between Obninsk, Russia and Pasadena, California. While we do not have a reliable measurement under California, our regional average in the western Eurasia (10-15 km thicker than the global average) is comparable with the estimate from their study (252 km). The thickened transition zone under this region may result from the effect of phase transitions under lower temperatures, as evidenced by fast velocities above and within the transition zone.

We further divide our measurements according to the regionalization scheme of Jordan (1981). The average perturbation in each tectonic regime is shown in Figure 5b. We observe a notable continent-ocean difference: the transition zone is on average 5-7 km thicker under stable continents than oceans. If we assume the slopes of the phase boundaries from a *Fo90* mantle composition, this thickness variation would translate to a difference in temperature of $40 - 60°C$. The thickness of the transition zone, does not correlate with the age of crust. The transition zone under subduction and orogenic regions is $\sim$10 km thicker than that under intermediate-age oceans. The thick transition zone under tectonic regions mainly results from a large-scale increase in thickness near the western Pacific subduction zones (Figure 5c), which may be related to the thermal effect of the flattening and accumulation of subducted oceanic lithosphere.

6. Discussion

It is not the aim of this study to image the topography of individual upper mantle discontinuities as earlier studies have done using SS precursors. Instead, our modeling approach is designed to provide a less velocity-dependent measure for the thickness of the transition zone, using a significantly improved SS precursor data set. In view of a recent debate, we focus on the long-wavelength features and the global variability of the transition zone thick-

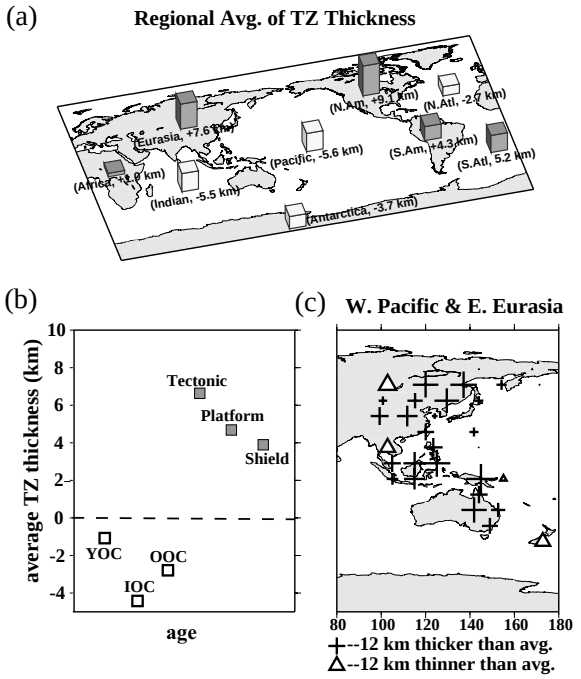

Figure 5: (a) Regionally averaged thickness of the transition zone. Positive values represent thicker than average transition zone, and negative values, thinner than average. (b) Average thickness of the transition zone for the 6 tectonic regions according to the regionalization scheme of Jordan (1981). The red symbols (below global average) are defined as: YOC – young ocean, IOC – intermediate aged ocean, and OOC – old ocean. A significant continent-ocean difference is observed, although transition zone thickness does not appear to correlate with the age of the crust. (c) Transition zone thickness under the western Pacific, which contributes significantly to the anomalously thick tectonic regions; this implies a significant thermal effect.

ness. The resolution of our approach is constrained by the wavelengths of the SS precursors (1500–2000 km laterally), and thus is slightly larger than the lateral resolution of recent tomographic studies.

Thickness variations inferred from our global measurements of $S410S - S660S$ are inconsistent with a "flat" transition zone; peak-to-peak variations of more than 25 km are observed. The large-scale features of our measurements are generally consistent with those of Flanagan and Shearer (1998) and Gu et al. (1998), and a low-pass filtration of our cap-averages shows comparable global pattern and variability with the results of Gossler and Kind (1996). However, the thickness variations observed in this study are much greater than those of Chevrot et al. (1999; less than 10 km). It is not clear if such departure results from differences in data coverage, measurement uncertainties, or data sensitivities to boundary perturbations. It is possible that some of the observations in Chevrot et al. (1999) are significantly affected by their choices of the P and S velocity models; another reason why our approach is preferable. In addition to velocity models, differences in the size of the Fresnel zones between the SS precursors and PdS waves may also be a factor: the finer-scale variations observed by Chevrot et al. (1999) are mostly averaged out in our study. It is conceivable that due to the small-scale nature of short-period PdS waves and the relatively sparse global coverage, some of the strongest local variations are left unimaged by Chevrot et al. (1999), in a laterally complex transition zone. For example, recent PdS wave studies on Hawaiian plume (Li et al. 2000a) and Japan subduction zone (Li et al. 2000b) show differential time variations from less than 19 s to more than 26.5 s (from 210 km to 280 km), over distances of a few hundred kilometers.

Our globally averaged thickness of the transition zone is 241.7 km; this agrees well with estimates from earlier studies of SS precursors, but is approximately 8 km thinner than that of Chevrot et al. (1999) (250 km). Part of the discrepancy with the latter study could be understood in terms of the locations of the measurements since the majority of the reported thickness values from that study are continental which are, on average, thicker in this study.

We observe a modest anticorrelation between the thickness variations of the transition zone and the temperature variations within the transition zone. This implies a considerable thermal influence to the boundary undulations of the transition zone discontinuities. Our global thickness perturbations are dominated by low-degree harmonics, particularly degree 2, which is also the strongest signature in the topography of the 660-km discontinuity (Shearer, 1993) and the lateral heterogeneities within the transition zone (Masters et al. 1982; Su et al. 1994; Gu et al. 2001). This correlation at degree 2 may imply a strong contribution to the thickness variations from the temperature-dependent topography of the 660-km discontinuity, particularly near the major subduction zones. In comparison, contribution from the topography of the 410-km discontinuity are less pronounced due to smaller variations at the boundary (Gu et al. 1998); this is reflective of a possible tradeoff between thermal and kinematic effects that are associated with the positive Clapeyron slope of the olivine α-to-β phase transition (Yuen et al. 1994; Thoraval and Machetel, 2000).

Finally, examination of the transition zone thickness variation shows a notable continent-ocean difference, i.e., the transition zone is on average 5–7 km thicker under continents than oceans. We do not observe, however, a

correlation between the thickness of the transition zone and the age of crust.

7. References

Chevrot, S., L. Vinnik, and J.-P. Montagner (1999), Global-scale analysis of the mantle *Pds* phases, J. Geophys. Res., 104, 20,203-20,219.

Dueker, K. G., and A. F. Sheehan (1997), Mantle discontinuity structure from midpoint stacks of converted P to S waves across the Yellowstone hotspot track, J. Geophys. Res., 102, 8313-8327.

Dziewonski, A. M., and D. L. Anderson (1981), Preliminary reference Earth model, Phys. Earth Planet. Inter., 25, 297-356.

Dziewonski, A. M., and F. Gilbert (1976), The effect of small, aspherical perturbations on travel times and a re-examination of the corrections for ellipticity, Geophys. J. R. Astron. Soc., 44, 7-17.

Flanagan, M. P., and P. M. Shearer (1998), Global mapping of topography on transition zone velocity discontinuities by stacking SS precursors, J. Geophys. Res., 103, 2673-2692.

Gossler, J., and R. Kind (1996), Seismic evidence for very deep roots of continents, Earth Planet. Sci. Lett., 138, 1-13.

Gurrola, H., and J. B. Minster (1998), Thickness estimates of the upper-mantle transition zone from bootstrapped velocity spectrum stacks of receiver functions, Geophys. J. Int., 133, 31-43.

Gu, Y. J., and A. M. Dziewonski (2001), Global variability of transition zone thickness, J. Geophys. Res. submitted.

Gu, Y., A. M. Dziewonski, and C. B. Agee (1998), Global de-correlation of the topography of transition zone discontinuities, Earth Planet. Sci. Lett., 157, 57-67.

Gu, Y. J., A. M. Dziewonski, W.-J. Su, and G. Ekström (2001), Models of the Mantle Shear Velocity and Discontinuities in the Pattern of Lateral Heterogeneities, J. Geophys. Res., 106, 11169-11199.

Jordan, T. H. (1981), Global tectonic regionalization for seismological data analysis, Bull. Seismol. Soc. Am. 71, 1131-1141.

Li, X., R. Kind, K. Priestley, S. V. Sobolev, F. Tilmann, X. Yuan, and M. Weber (2000a), Mapping the Hawaiian plume with converted seismic waves, Nature, 405, 938-941.

Li, X., S. V. Sobolev, R. Kind, X. Yuan, and Ch. Estabrook (2000b), A detailed receiver function image of the upper mantle discontinuities in the Japan subduction zone, Earth Planet. Sci. Lett., 183, 527-541.

Masters, G., T. H. Jordan, P. G. Silver, and F. Gilbert (1982), Aspherical Earth structure from fundmental spheroidal-mode data, Nature, 298, 609-613.

Shearer, P. M. (1993), Global mapping of upper mantle reflectors from long-period SS precursors, Geophys. J. Int., 115, 878-904.

Shearer, P. M., and T. G. Masters (1992), Global Mapping of topography on the 660-km discontinuity, Nature, 355, 791-796.

Su, W.-J., R. L. Woodward, and A. M. Dziewonski (1994), Degree-12 model of shear velocity heterogeneity in the mantle, J. Geophys. Res., 99, 6945-6980.

Thoraval, C., and P. Machetel (2000), Accounting for phase changes and their kinetics within geodynamic model for the geoid, EOS, Trans. Am. Geophys. Soc. Suppl., 81, F1240.

Wicks, C. W., and M. A. Richards (1993), A detailed map of 660-kilometer discontinuity beneath the Izu-Bonin subduction zone, Science, 261, 1424-1427.

Yuen, D. A., D. M. Reuteler, S. Balachandar, V. Steinbach, A. V. Malevsky, and J. J. Smedsmo (1994), Various influences on three-dimensional mantle convection with phase transitions, Phys. Earth Planet. Inter., 86, 185-203.